16th Australasian Fluid Mechanics Conference
Crown Plaza, Gold Coast, Australia
2-7 December 2007

A Forecast Model for Atmospheric Internal Waves Produced by a Mountain

J. W. Rottman[1], D. Broutman[2] and S. D. Eckermann[3]

[1]Naval Hydrodynamics Division
Science Applications International Corporation
10260 Campus Point Drive, San Diego, CA 92121 USA

[2]Computational Physics, Inc.
8001 Braddock Road, Springfield, VA, 22151, USA

[3]Space Science Division
Naval Research Laboratory
Washington DC.

Abstract

Fourier synthesized ray solutions are an effective way to model mountain waves, producing fast high-resolution three-dimensional forecasts. Here this method is extended to include tunneling effects, i.e. the penetration of mountain waves through an evenescent region bounded above and below by turning points. Tunneling effects are especially important near wind jets. To overcome the divergence of ray theory at the turning points, without resorting to special functions, the ray solution is linearly interpolated across the turning point region. A comparison of the ray solution with a mesoscale model indicates the importance of including a wind curvature term in the ray analysis.

Introduction

Mountain waves are internal gravity waves generated by stratified flow over topography. These waves can grow to large amplitudes as they propagate upward to great heights in the atmosphere, resulting in strong vertical accelerations and wavebreaking. Forecasting mountain waves is thus important for aviation safety and a host of scientific issues, including mixing rates for stratospheric ozone.

Here we use Fourier synthesized ray solutions to forecast mountain waves in a height dependent background. Ray solutions are first obtained in a Fourier transform domain, where the wave propagation is governed by one-dimensional height-dependent ray equations. The result is then converted to a three-dimensional spatial solution by inverse Fourier transform

Previous work with this method (Broutman et al. 2003, Eckermann et al. 2006) treated trapped waves with an Airy function analysis. This is appropriate for an isolated turning point, and it predicts the complete reflection of the wave from the turning point. If there are two nearby turning points, however, up to half of the wave's momentum flux can leak through the evanescent region between the two turning points and continue upward with the transmitted wave. This process is especially important near wind jets. It is analagous to tunneling in quantum mechanics (Brown and Sutherland 2007).

Here we examine two turning-point effects. We introduce a modified ray solution, which is linearly interpolated across the turning point region where ray theory breaks down. This is computationally fast, which is important because in practical applications of this method thousands of rays can encounter closely spaced turning points. We compare the modified ray solution with a uniformly valid solution and a numerical integration of the vertical eigenfunction equation. We also find that including a wind curvature term in the ray analysis leads to better agreement with a mesoscale model simulation.

The method

We examine stationary mountain waves propagating in a background that depends on the height z only. The mean wind has components $U(z), V(z)$ in the horizontal x, y directions, respectively. The mean buoyancy frequency is $N(z)$. We work in terms of the vertical velocity $w(x,y,z)$ and its vertical eigenfunction $\tilde{w}(k,l,z)$, where k,l is the horizontal wavenumber vector.

The vertical eigenfunction $\tilde{w}(k,l,z)$ satisfies (Shutts and Broad 1993)

$$\tilde{w}_{zz} + (l_s^2 - k_h^2)\tilde{w} = 0\,, \tag{1}$$

where $k_h^2 = k^2 + l^2$, and l_s is the Scorer parameter defined by

$$l_s^2 = N^2/\bar{U}^2 - \bar{U}_{zz}/\bar{U}\,. \tag{2}$$

Here $\bar{U}(z)$ is the wind component in the direction of the horizontal wavenumber vector (k,l).

The spatial solution w is obtained from $\tilde{w}$ by the inverse Fourier transform

$$w(x,y,z) = e^{z/2H_0} \iint_{-\infty}^{\infty} \tilde{w}(k,l,z)\, e^{i(kx+ly)} dk\, dl\,, \tag{3}$$

where $H_0 \simeq 7.5$km is the density scale height.

By Fourier synthesized ray solutions, we mean the Fourier synthesis (3) of the the ray solutions to (1). These ray solutions involve phase integrals of the form $\exp(i\int m dz)$, where the vertical wavenumber m is defined by the dispersion relation

$$m^2 = N^2/\bar{U}^2 - k_h^2\,. \tag{4}$$

The wind curvature term $\bar{U}_{zz}/\bar{U}$ in (2) is ignored in the ray approximation, since $\bar{U}$ is assumed to be slowly varying over the vertical distance of m^{-1}. However, the wind curvature term can be important for waves with turning points near the tip of a wind jet, as we show below. An anelastic correction to the dispersion relation (4) involving H_0 was found to be unimportant in the examples considered here.

Our notation is such that m is postive/negative for upgoing/downgoing wave groups. This is opposite to the usual notation for internal gravity waves, but it is standard for two turning-point theories developed for other applications and applied here.

Figure 1 illustrates the problem. A wind jet produces an evanescent region ($m^2 < 0$) between the turning point heights z_1 and

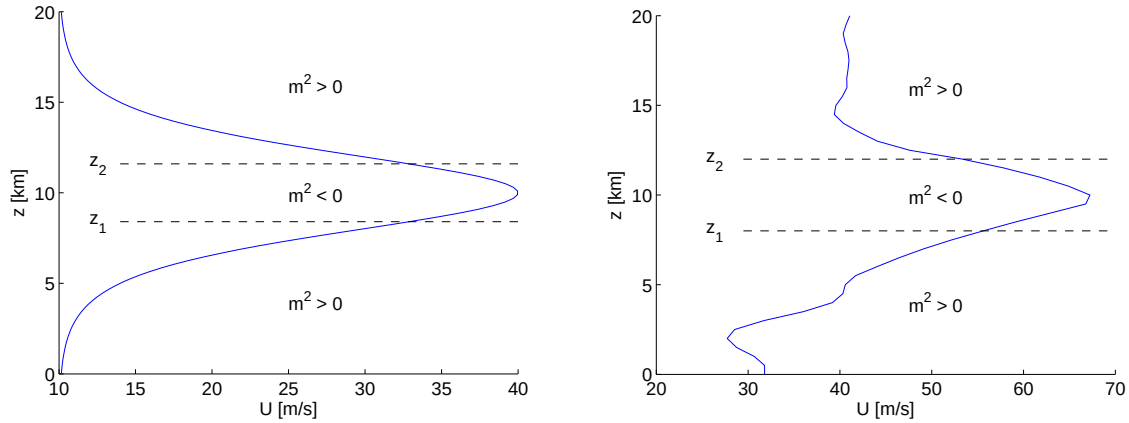

Figure 1: Wind profiles used in the present paper. Left panel: A $\mathrm{sech}^2(z)$ wind profile. Right panel: The wind profile obtained from radiosonde measurements and used in Eckermann et al. (2006). The waves have turning points at the have heights z_1 and z_2, which for a given background are functions of the horizontal wavenumber of the waves.

z_2, surrounded by propagating regions ($m^2 > 0$) above and below. The heights z_1, z_2 occur where $m^2 = 0$ and depend through (4) on the horizontal wavenumbers k, l and the background stratification and wind profiles. An incident wave launched from $z = 0$ propagates upward toward the lower turning point at $z = z_1$, generating a reflected wave propagating downward below z_1 and a transmitted wave propagating upward above z_2.

We first derive solutions for $\tilde{w}$ in an unbounded region. We then introduce a lower boundary at $z = 0$, representing the ground, and account for repeated reflections between the ground and lower turning point.

The ray solution is derived by Froman and Froman (1970) and involves the phase integrals

$$q_1(z) = \int_{z_1}^{z} m\,dz, \tag{5}$$

$$q_2(z) = \int_{z_2}^{z} m\,dz, \tag{6}$$

$$Q = \int_{z_1}^{z_2} |m|\,dz. \tag{7}$$

Note that for $z < z_1$, we have from (5) negative q_1 but positive dq_1/dz. Thus in the following ray solutions we associate $\pm q_1$ with, respectively, upgoing and downgoing wave groups below the lower turning point.

The ray solutions are

$$\tilde{w}_t = Cm^{-1/2} e^{i(q_2+\pi/4)}, \tag{8}$$

$$\tilde{w}_r = C|m|^{-1/2} e^{Q} e^{-i(q_1+\pi/4)}, \tag{9}$$

$$\tilde{w}_i = Cm^{-1/2}[e^{2Q}+1]^{1/2} e^{i(q_1+\pi/4+2\sigma)}, \tag{10}$$

where C is a constant. The subscripts t, r, i refer, respectively, to the transmitted wave (defined for $z > z_2$), and the reflected and incident waves (defined for $z < z_1$). An expression for σ is derived by Froman and Dammert (1970), given by their eq. (57) as

$$\sigma = .5\,[Q^* \log Q^* - Q^* + \arg\Gamma(.5 - iQ^*)] \tag{11}$$

where $Q^* = Q/\pi$.

The ray solution for $\tilde{w}$ is

$$\tilde{w}(z) = \tilde{w}_i + \tilde{w}_r \quad z < z_1 \tag{12}$$

$$\tilde{w}(z) = \tilde{w}_t \quad z > z_2 \tag{13}$$

The upper boundary condition is a radiation condition, satisfied by the form chosen for $\tilde{w}_t$, which represents an outgoing wave. Between the two turning points, where m is imaginary, we use (Froman and Froman 1965)

$$\tilde{w}(z) = C|m|^{-1/2} e^{-|q_2|} \quad z_1 < z < z_2. \tag{14}$$

Uniformly valid solution

The ray solution for $\tilde{w}$ diverges at a turning point, where $m = 0$. A uniformly valid solution that corrects the ray singularity at two turning points involves Weber functions (related to parabolic cylinder functions). It has the form (Kravtsov and Orlov 1999)

$$\tilde{w}(z) = DA(z)\,E(b, \zeta(z)), \tag{15}$$

where E is the Weber function, D is a constant, and

$$A(z) = [(\zeta^2(z) - b^2)/m^2(z)]^{1/4}, \tag{16}$$

$$b = 2Q/\pi. \tag{17}$$

The mapping $\zeta(z)$ is defined by an integral equation that is solved iteratively and depends on phase integrals similar to (5)-(7). Note that A is proportional to $m^{-1/2}$, as is the ray solution. But A remains finite at a turning point, because the two turning points occur at $\zeta = \pm b$. For further details, see Kravtsov and Orlov (1999).

Eigenfunction approximations for a sech^2(z) wind profile

We first consider the wind profile shown in the left panel of Figure 1, given by

$$U = U_0 + U_1 \mathrm{sech}^2((z - z_m)^2/L^2) \tag{18}$$

with $U_0 = 10\,\mathrm{ms}^{-1}$, $U_1 = 30\,\mathrm{ms}^{-1}$, $z_m = 10\,\mathrm{km}$, and $L = 3\,\mathrm{km}$. The other background parameters are $V = 0$ and $N = 0.015\mathrm{s}^{-1}$.

Figure 2 shows the real and imaginary parts of the ray and uniform solutions of (1), along with a solution by numerical integration (see below). These were computed at 100 evenly spaced

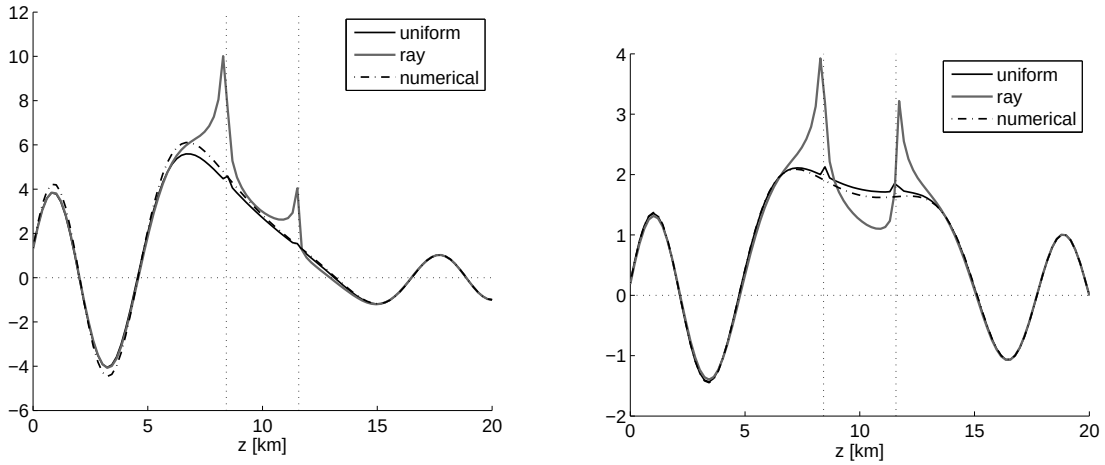

Figure 2: The real (left panel) and imaginary (right panel) parts of the solution $\tilde{w}$ for the wind profile (18). Vertical dotted lines indicate the turning point locations, at $z_1 \simeq 8.4\,\mathrm{km}$ and $z_2 \simeq 11.6\,\mathrm{km}$. The horizontal wavelength of the waves is about 13.8 km. The solutions are normalized so that $\tilde{w} = -1$ at $z = 20\,\mathrm{km}$.

heights from 0 to 20 km. The ray solution diverges at both turning points (vertical dashed lines), though the computed values remain finite because the discrete grid misses the turning points slightly. The curve for the uniform solution shows a small notch near the turning points, most noticeably in the right panel of the figure. These occur because of roundoff error in the calculation for $A(z)$ in (16), which is the quotient of two terms that vanish at the turning points.

The numerical solution to (1) was calculated with a Runge-Kutta method using an initial condition given by the the transmitted ray solution (8) at $z = 20\,\mathrm{km}$. This was then integrated downward to $z = 0$. The numerical solution begins to separate slightly from the uniform solution as the integration proceeds down into the evanescent region between the turning points. For the real part of $\tilde{w}$, the numerical solution is slightly larger in amplitude than the uniform solution at heights below z_1.

The modified ray solution

In practice, mountain wave forecasts involve the calculation of $\tilde{w}(k,l,z)$ for tens of thousands of k,l values. Thus we would like to use the ray method, which is much faster than the uniform and numerical methods. To do so, we need an efficient way to correct the ray theory breakdown near the two turning points.

We first identify the region of ray-theory breakdown near the turning points using the following quantity (Froman and Froman 1965), which measures the slow variation of the vertical wavenumber m:

$$\varepsilon = \frac{1}{|m|^2}\left|\frac{3}{4}\left(\frac{1}{m}\frac{dm}{dz}\right)^2 - \frac{1}{2m}\frac{d^2m}{dz^2}\right| \tag{19}$$

$$= \frac{1}{16m^6}\left|5\left(\frac{dm^2}{dz}\right)^2 - 4m^2\frac{d^2m^2}{dz^2}\right|. \tag{20}$$

Ray methods are asymptotically valid, i.e. their accuracy improves as $\varepsilon \to 0$. At a turning point ε diverges, since neighboring rays with slightly different values of m cross each other. This results in a divergence of dm/dz and the other derivatives in the above expressions.

We consider ray theory to be sufficiently accurate wherever $\varepsilon < 1$, and we leave the ray solution as it is in those regions. In a region where $\varepsilon > 1$ we replace the ray solution with linear interpolated values across that region. Let $z = r$, $z = s$ be heights on either side of a region where $\varepsilon = 1$. Our modification to the ray solution is then given by the linear interpolation

$$\tilde{w}(r < z < s) \to \tilde{w}(r) + (z-r)\,\frac{\tilde{w}(s) - \tilde{w}(r)}{s-r}\,. \tag{21}$$

We show examples of this modification (indicated by heavy dashed lines) in Figure 3. The two upper panels are the same cases as the corresponding panels of Figure 2. The bottom two panels show results for more closely spaced and more widely spaced turning points. We approximated ε using centered differences for the derivatives of m^2 in (20). For the upper panels, $\varepsilon > 1$ at heights between 6.8 and 9.7 km, and between 10.3 and 13.1 km. The ray solution in these height ranges is replaced by the linear interpolation in (21).

The upper right panel of Figure 3 shows that occassionally the modified ray method is not so accurate. Here ε reaches a minimum of 0.72 near the middle of the wind jet at $z = 10\,\mathrm{km}$, and yet the ray solution is not accurate there. We expermented with other values of ε for determining ray theory validity, but the value of unity consistently led to the best approximation. A possible improvement to our procedure would be to interpolate across the entire evanescent region whenever the two turning points are close together, as judged by the integral Q of (7) being less than a certain value, say unity. In this example $Q \simeq 0.64$. We may consider this possibility in future applications.

Lower boundary condition and wave transience

Mountain waves that reflect from a turning point return to the ground where they reflect upward again. We have not yet taken into account the contribution from these ground reflected waves. A way to do so is outlined in the Broutman et al. (2006) and is summarized here.

Each reflection from the ground generates a new incident wave, with a phase shift and a change in amplitude relative to the original incident wave. The phase shift is due to the total phase change in propagating from the ground to the lower turning point and then back to the ground again, including the phase shift of $-\pi/2$ for reflection at the turning point and the phase shift of π for reflection at the ground. The total phase shift is

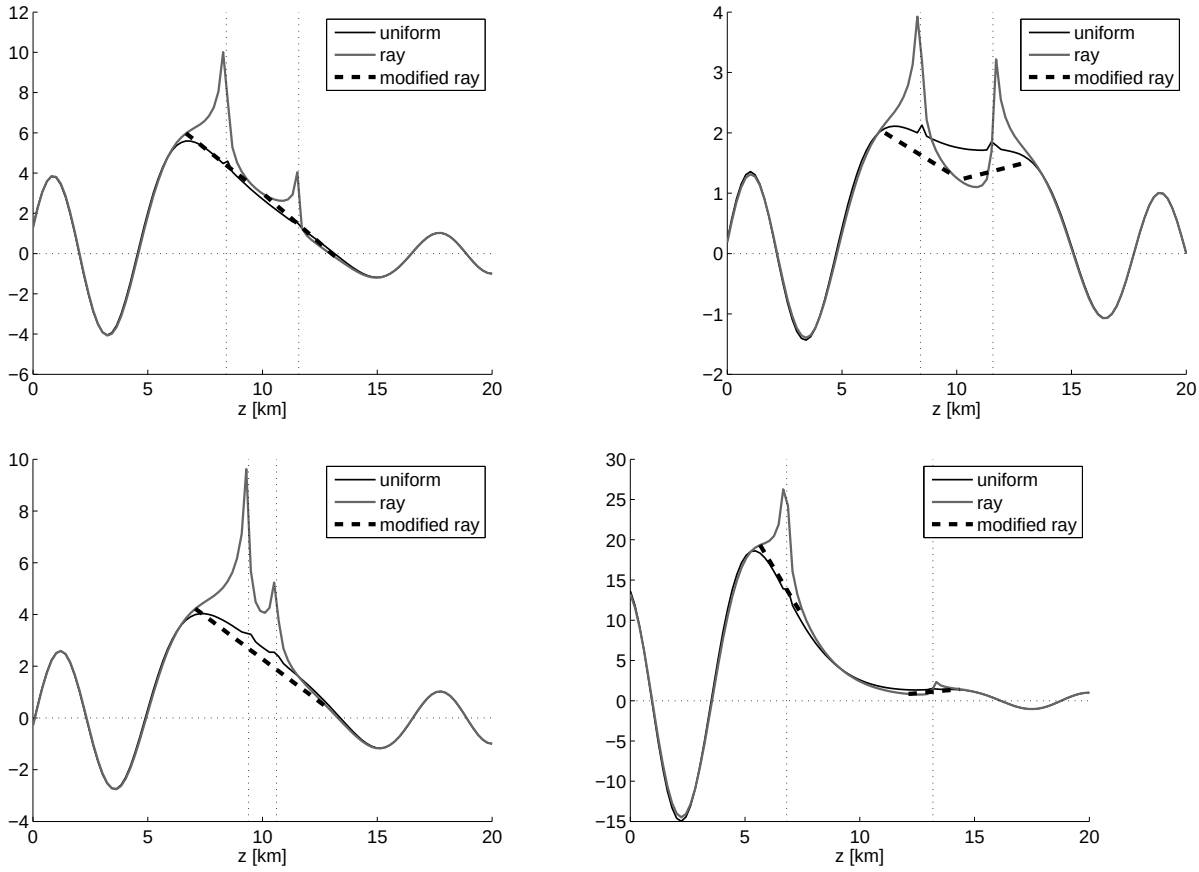

Figure 3: The modified ray solution, obtained by linear interpolation across the turning point regions and denoted by the dashed line. Upper panels: the same case as the corresponding panels in Figure 2. Also shown are examples with closely spaced turning points (lower left panel) and widely spaced turning points (lower right panel).

then

$$\Phi = 2\int_0^{z_1} m\,dz + \pi/2\,. \tag{22}$$

The change in amplitude is given by

$$R \equiv |w_r|/|w_i| = e^Q/(e^{2Q}+1)^{1/2}\,. \tag{23}$$

This reflection coefficient is the ratio of the ray amplitudes for the reflected and incident wave solutions of (9)-(10). As the distance between the two turning points widens, Q increases and R approaches unity.

To incorporate N_r reflections from the ground, we take the solutions for $\tilde{w}$ obtained above (ray, uniform, numerical) and multiply each by

$$S = \sum_{n=0}^{N_r} R^n e^{in\Phi}\,. \tag{24}$$

The number of ground reflections N_r depends on the propagtion time T from the ground to the lower turning point and back to the ground:

$$T = 2\int_0^{z_1} c_g^{-1}\,dz \tag{25}$$

where c_g is the vertical group velocity. At time t, the number of ground reflections can be approximated as t/T rounded to the nearest integer. This approach was tested by Broutman et al. (2006) and used by Eckermann et al. (2006).

Waves with one or no turning points.

To simulate the full spectrum of mountain waves, we also need the solution for waves that have one or no turning points. The solution for one turning point involves the Airy function. It is given in the Appendix of Eckermann et al (2006) and will not be repeated here. The solution for waves without turning points is

$$\tilde{w} = C_1|m|^{-1/2}e^{iq}\,. \tag{26}$$

where $q = \int_0^z m dz$ and C_1 is a constant.

There is a better approximation than (26) for waves that just miss having turning points. It is similar to the two-turning point ray solution (8)-(10), but the turning points have complex z values. Unlike (26) it accounts for partially reflected and partially transmitted waves. We are presently implementing that solution and hope to report some results derived from it in the future.

Mountain waves: an idealized case

We first consider a two-dimensional example, with the wind profile given by (18), and a constant $N = 0.015\text{s}^{-1}$. The topography is

$$h = h_0/(1+x^2/L^2) \tag{27}$$

with $h_0 = 100\,\text{m}$ and $L = 2.5\,\text{km}$. The linearized lower boundary condition is applied. This equates $\tilde{w}_i$ in (10) to $\tilde{h}$ at $z = 0$, where $\tilde{h}(k)$ is the Fourier transform of $h(x)$.

The left panel of Figure 4 shows the result obtained using the modified ray solution. This was calculated on a grid with a spacing of 1 km in x and 100 m in z. The dashed lines indicate the turning point heights for the resonant modes (see below).

The middle panel shows the result from the Weather Research and Forecasting (WRF) model, a mesoscale model described by Skamarock et al. (2005). This was computed on a 480 by 301 grid with a spacing of 250 m in x and 100 m in z. The WRF simulation includes a sponge layer that starts at $z = 20\,\text{km}$.

The right panel shows the result calculated the same way as for the left panel, except that the wind curvature term has been included in the dispersion relation. Thus (4) becomes

$$m^2 = N^2/\bar{U}^2 - \bar{U}_{zz}/\bar{U} - k_h^2\,. \tag{28}$$

Since we are considering a two-dimensional case, $\bar{U} = U$.

Including the wind curvature term has led to a better agreement with the WRF solution, particularly at heights in the range of about $6-10\,\text{km}$, where the left panel shows higher wave amplitudes than the middle and right panels.

To help explain these results, we consider the resonant modes. These have a phase change Φ in (22) that is a multiple of 2π, so there is perfect constructive interference between the reflected waves. The resonant horizontal wavelengths for the wind profile (18) are

$$\lambda \simeq 5.0\,,\ 7.2\,,\ 15.9\,\text{km}. \tag{29}$$

The corresonding heights of the lower turning point are

$$z_1 \simeq 3.9\,,\ 6.0\,,\ 9.2\,.\text{km} \tag{30}$$

These heights are indicated by dashed lines in the left panel of Figure 4, and in the middle panel to assist in comparing the results.

The above values were calculated without the wind curvature term. When wind curvature is included, we find only two resonant modes, with

$$\lambda \simeq 5.1\,,\ 7.5\,,\text{km} \tag{31}$$

and

$$z_1 \simeq 3.8\,,\ 5.8\,.\text{km} \tag{32}$$

Since $\bar{U}_{zz}$ is negative near the tip of the wind jet, the wind curvature term $-\bar{U}_{zz}/\bar{U}$ adds a postive contribution to m^2 and prevents it from vanishing for λ near 16 km. Thus we lose the resonant mode that has a turning point at $z_1 \simeq 9.2\,\text{km}$ and that results in the relatively large amplitudes in the $6-10\,\text{km}$ height range. These heights in (32) are indicated by dashed lines in the right panel of Figure 4.

Mountain waves: a realistic case

We present some preliminary results for mountain waves generated by the island of Jan Mayen, in the North Atlantic. This is for the wind profile shown in right panel of Figure 1, which has a strong wind jet centered at a height of about 10 km. The stratification profile, the topography, and other details are given in Eckermann et al. (2006).

Three solutions for w are presented in Figure 5. The calculations are three-dimensional, but only the vertical cross sections are shown here. The left panel is the solution based on a single turning-point theory involving Airy functions. This is the solution given in Eckermann et al. (2006). It reveals very little wave transmission above the 10 km wind jet.

The right panel of Figure 5 is from our modified ray solution. The wavefield above the wind jet is much stronger than in the left panel, and compares fairly well in magnitude with the WRF solution, pictured in the middle panel. However, the dominant

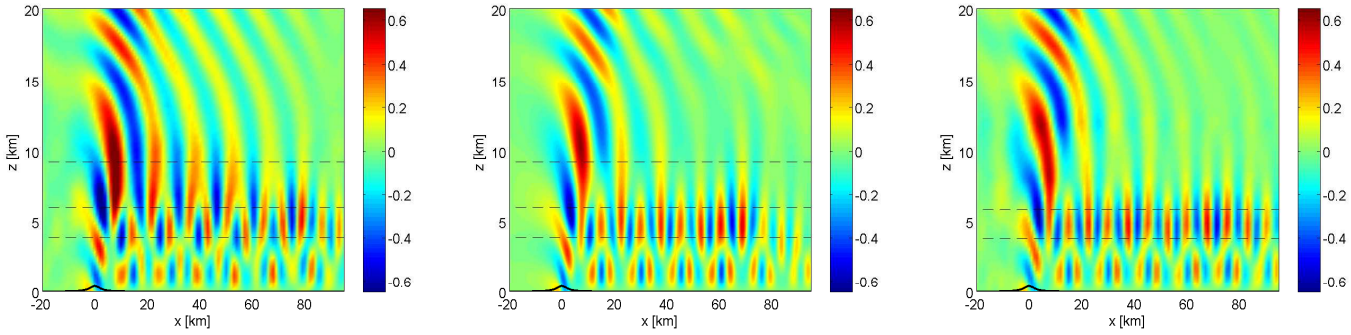

Figure 4: Left: modified ray solution without the wind curvature term. Middle: WRF solution. Right: modified ray solution with the wind curvature term. Colorbar values are for w in ms^{-1}. Dashed lines indicate the heights of the lower turning points for the resonant modes, from (30) for the left and middle panels, and from (32) for the right panel. The mountain profile (27) is shown, amplified by a factor of 4 for visibility.

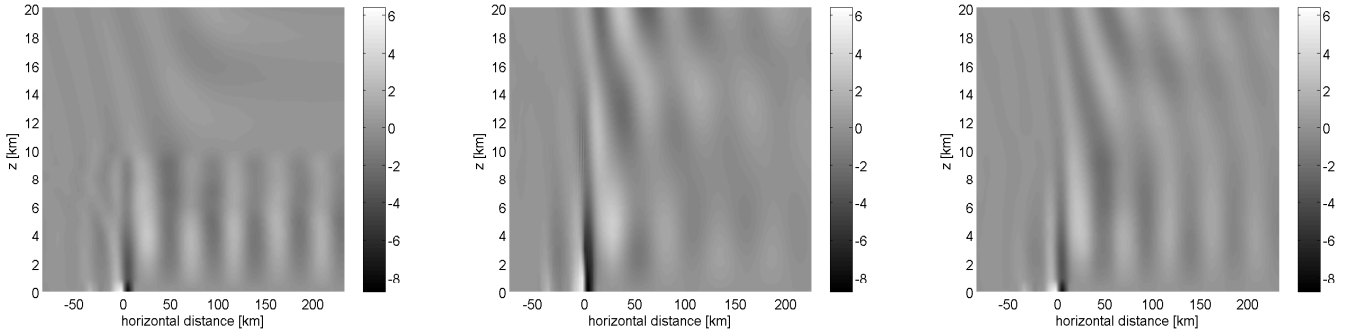

Figure 5: Mountain waves generated by Jan Mayen, in vertical cross section. Left: Airy function solution accounting for a single turning point only, as computed by Eckermann et al. (2006). Middle: WRF solution. Right panel: modified ray solution. Colorbar values are for w in ms^{-}1.

horizontal wavelength above the wind jet is somewhat shorter for the modified ray solution than for the WRF simulation. We have not yet included the effects of wind curvature in this calculation, which may be the source of this discrepancy.

Comments

We have demonstrated that Fourier synthesized ray solutions can effectively model mountain waves in the presense of two turning points caused by a wind jet. We dealt with the breakdown of ray theory near the turning points by linearly interpolating the ray solution across the turning point regions, as illustrated in Figure 3. We tested the accuracy of this modified ray approach by comparing its predictions with a uniformly valid theory and a numerical integration of the vertical eigenfunction equation, both of which require much longer computation times.

The results can be sensitive to the effects of wind curvature in the dispersion relation, especially if a resonant mode has a turning point near the tip of a wind jet (see Figure 4).

Acknowledgements

We thank John Lindeman and Jun Ma for providing the WRF results.

References

[1] Broutman, D., Rottman, J.W., Eckermann, S.D. 2003 A simplified Fourier method for nonhydrostatic mountain waves. *J. Atmos. Sci.* **60** 2686–2696.

[2] Broutman, D., J. Ma, S.D. Eckermann, and J. Lindeman, 2006: Fourier-ray modeling of transient trapped lee waves. *Mon. Wea. Rev.*, **134**, 2849–2856.

[3] Brown, G.L., and B.R. Sutherland, 2007: Internal wave tunnelling through non-uniformly stratified shear flow. *Atm.-Ocean*, **45**, 47–56.

[4] Eckermann, S.D., D. Broutman, J. Ma and J. Lindeman, 2006: Fourier-ray modeling of short wavelength trapped lee waves observed in satellite imagery near Jan Mayen. *Mon. Wea. Rev.*, **134**, 2830–2848.

[5] Fröman, N., and P.O. Fröman, 1965: JWKB Approximation. North Holland, 138pp.

[6] Fröman, N., and P.O. Fröman, 1970: Transmission through a real potential barrier by means of certain phase-integral approximations. *Nucl. Phys.*, **A147**, 606–626.

[7] Fröman, N., and Ö. Dammert, 1970: Tunneling and superbarrier transmission through a system of two real potential barriers. *Nucl. Phys.*, **A147**, 627–649.

[8] Kravtsov, Y.A, and Y.I Orlov (1999): Caustics, Catastrophes, and Wave Fields. Springer, 216pp.

[9] Shutts, G., and A. Broad, 1993: A case study of lee waves over the Lake District in Northern England. *Quart. J. Roy. Met. Soc.***199**, 377–408.

[10] Skamarock, W.C., Klemp, J.C., Dudhia, J., Gill, D.O., Barker, D.M., Wang, W., Powers, J.G. 2005 A description of the advanced research WRF version 2. *NCAR Technical Note*, Boulder, CO, USA.